Electronic Supplementary Information for

Simple dimer containing dissociatively-stable mono-imidazole ligated ferrohemes

Q. Yang, D. Khvostichenko, J. Atkinson and R. Boulatov

1. Syntheses and characterization.

All reagents were used as supplied commercially unless otherwise noted. Metallation of free-base porphyrins with Fe^{II} and handling of Fe^{II}-porphyrins were done in a drybox under an atmosphere of N_2 with <1 ppm O_2 and H_2O, using rigorously dried and deoxygenated solvents and liquid reagents. The latter was established by spectrophotometric testing with Na benzophenoneketyl. NMR spectra were recorded on a 500 MHz Unity-INOVA Varian spectrometer at 25°C. UV-vis spectra were recorded on Varian Cary 50 spectrometer using a fiber optic dip probe or in a sealed cuvette.

Free-base porphyrins **1**H_2, **2**H_2 and **3**H_2 were synthesized according to previously described procedures[1] The free bases were metalated with Fe by stirring a solution of the free base, $FeBr_2$ (1.2 eq.) and 2,6-lutidine (10 eq) in toluene/thf (1:1) at room temperature overnight. The reaction mixtures were dried under vacuum for 24 hours to remove all traces of 2,6-lutidine, redissolved in toluene (for (**1**Fe)$_2$) or toluene/thf (1:1 for **2**Fe and **3**Fe) and filtered through a 1 cm plug of activated neutral alumina to remove the lutidinium salt and excess $FeBr_2$. The use of thf for **2**Fe and **3**Fe was necessary due to the high polarity of the pyridine moiety. In contrast, dimerization of **1**Fe yielded non-polar (**1**Fe)$_2$, which could be eluted off alumina with toluene. The syntheses were carried out on a ~50 mg scale and *isolated* yields were >90% for (**1**Fe)$_2$ and ~80% for **2**Fe and **3**Fe (losses were due to incomplete elution off the alumina, which was done intentionally to ensure the complete removal of unreacted $FeBr_2$ from the samples). The ^{1}H-NMR spectra of (**1**Fe)$_2$(PhNO)$_2$, (**1**Fe)$_2$(^{i}PrNC)$_2$ in $CDCl_3$, and **2**Fe and **3**Fe in pyridine-d_5 are tabulated in Table S1 along with that of **1**H_2, to illustrate the upfield shift in the imidazole and β-pyrrolic signals upon metallation with Fe, which is indicative of dimerization. Solutions of (**1**Fe)$_2$, **2**Fe and **3**Fe in $CDCl_3$ under 1 atm of CO remained paramagnetic, precluding the NMR characterization of these ferrohemes as CO adducts, which is a standard practice in Fe(II) porphyrin chemistry. Solutions of Fe(tpp) (tpp = tetraphenylporphyrin) in $CDCl_3$ under 1 atm of CO are also paramagnetic. The UV-vis spectra are shown in Figure S1. MS (ES): (**1**Fe)$_2$, m/e: 1225.8 (calculated for (**1**Fe)$_2$+1, $C_{72}H_{80}Fe_2N_{12}$: 1225.5); **2**Fe, m/e: 610.8 (calculated for **2**Fe+1, $C_{37}H_{39}FeN_5$: 610.3); **3**Fe, m/e: 838.1 (calculated for **3**Fe+1, $C_{55}H_{51}FeN_5$: 838.4). We were unable to obtain satisfactory elemental analyses, probably due to partial oxidation of the complexes during sample preparation by the analytical lab and formation of Fe carbides during combustion: elemental analyses of metalloporphyrins are rarely successful.

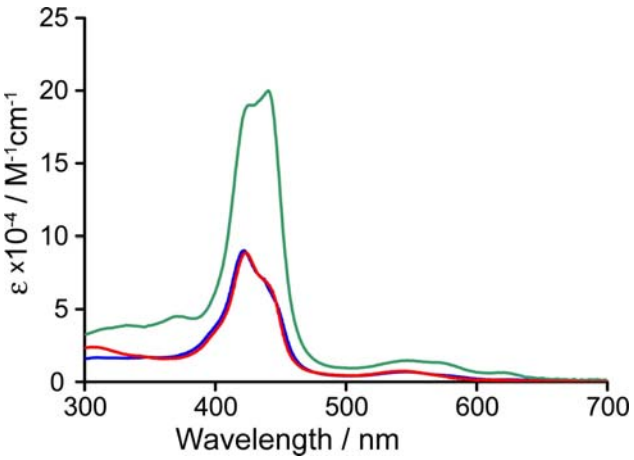

Figure S1. Absorption spectra of (**1**Fe)$_2$ (green), **2**Fe (red) and **3**Fe (blue) in toluene at 50 μM; λ_{max}, nm ($\varepsilon\times10^{-4}$, $M^{-1}cm^{-1}$): (1Fe)2, 373 (4.5), 429 (19), 441 (20), 548 (1.5), 575 (1.3), 625 (0.6); 2Fe: 420 (9), 442 (sh), 545 (0.7); 3Fe: 422 (9), 545 (0.7), 580 (0.3).

[1] (a) Stibrany, R. T.; Vasudevan, J.; Knapp, S.; Potenza, J. A.; Emge, T.; Schugar, T. J. *J. Am. Chem. Soc*. **1996**, *118*, 3980. (b) Geier, G. R.; Lindsay J. S. *Tetrahedron* **2004**, *60*, 11435.

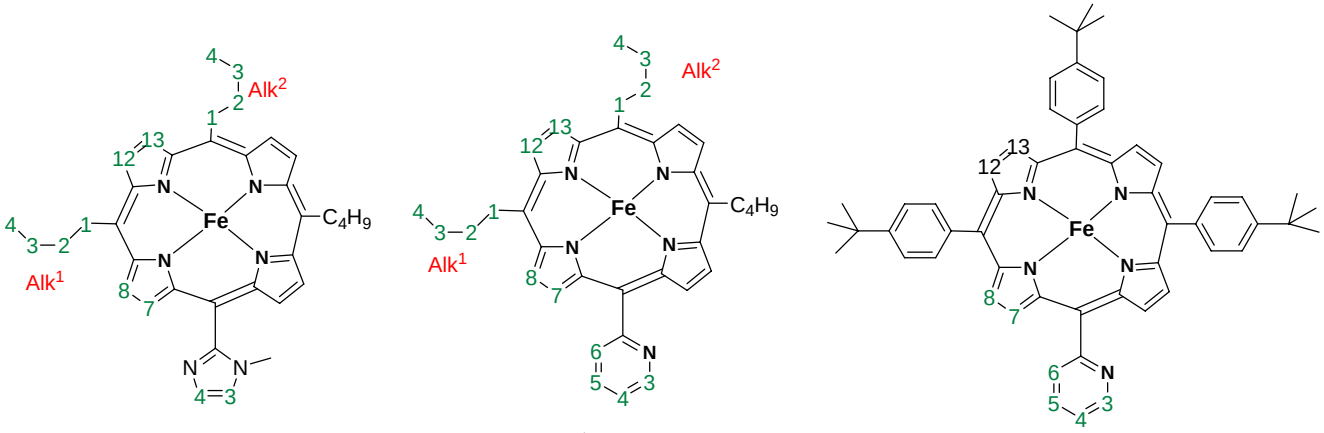

Figure S2. Numbering scheme for assignment of ^{1}H-NMR spectra.

Table S1. ^{1}H-NMR shifts; solutions in $CDCl_3$, unless noted otherwise.

	1H_2	(**1**Fe)$_2$(PhNO)$_2$	(**1**Fe)$_2$(^{i}PrNC)$_2$	(**1**Fe)(^{i}PrNC)	**2**Fe[a]	**3**Fe[a]
β-pyrrolic						
7	8.81 (d, 3 Hz)	5.49 (d, 4.6 Hz)	5.60	8.88 (d, 5 Hz)	8.7[b]	8.82 (d,
8	9.52 (d, 5 Hz)	8.75 (d, 5 Hz)	8.97	9.25 (d, 5.2 Hz)	9.42 (d, 5 Hz)	9.0 (d, 4.8 Hz)
12	9.46 (d, 5 Hz)	9.47 (d, 5 Hz)	9.58 (d, 3.8 Hz)	9.38 (d, 5 Hz)	9.52 (d, 5 Hz)	8.89 (d, 4.5 Hz)
13	9.46 (d, 5 Hz)	9.60 (d, 4 Hz)	9.72 (d, 4 Hz)	9.40 (d, 5 Hz)	9.55 (d, 5 Hz)	
imidazole						
3	7.43	4.69 (d, 1.7 Hz)	2.06	6.97 (d, 1.2 Hz)		
4	7.75	2.04 (d, 1.6 Hz)	2.96	7.81 (d, 1.3 Hz)		
Me	3.35	1.74	1.30	3.08		
pyridine						
3					8.17 (dt, 7.6 Hz, 1.2 Hz)	8.26 (dt, 1, 7.6 Hz)
4					8.08 (td, 7.6 Hz, 1.9 Hz)	8.09 (td, 1.8 Hz, 7.8 Hz)
5					7.71 (ddd, 1.2 Hz, 5 Hz, 7.6 Hz	7.70 (dd, 1 Hz, 7.8 Hz)
6					9.13 (ddd, 1 Hz, 1.9 Hz, 5 Hz)	9.15 (dm, 5 Hz)
peripheral substituents						
Alk^1-1	4.89 (t, 8 Hz)	4.85, 4.75 (m)	4.89, 5.00 (m)	4.69 (m)	4.96 (dd, 6.7 Hz, 10 Hz)	
Alk^1-2	2.56 (m)	2.54 (m)	2.80 (m)	2.48 (m)	2.49 (m)	
Alk^1-3	1.85 (six, 7.5 Hz)	1.82 (m)	1.96 (m)	1.62 (m)	1.79 (six, 7.6 Hz)	
Alk^1-4	1.21 (t, 7.5 Hz)	1.15 (t, 7.5 Hz)	0.62 (br. s)	0.99 (t, 7.4)	1.11 (t, 7.4 Hz)	
Alk^2-1	4.94 (t, 8 Hz)	4.95 (m)	5.14 (m)	4.78 (m)	5.02 (dd, 6.9 Hz, 11 Hz)	

	1H_2	(**1**Fe)$_2$(PhNO)$_2$	(**1**Fe)$_2$(^{i}PrNC)$_2$	(**1**Fe)(^{i}PrNC)	**2**Fe[a]	**3**Fe[a]
Alk^2-2	2.56 (m)	2.71 (m)	2.90 (m)	2.56 (m)	2.56 (m)	
Alk^2-3	1.85 (six, 7.5 Hz)	1.92 (m)	1.96 (m)	1.67 (m)	1.86 (six, 7.5 Hz)	
Alk^2-4	1.22 (t, 7.5 Hz)	1.24 (t, 7.5 Hz)	0.62 (br. s)	1.02 (t, 7.5 Hz)	1.17 (t, 7.4 Hz)	
Ph						8.15 (m), 7.60 (m)
^{t}Bu						1.64
exogenous ligand		*o*: 2.25 (d, 8.3 Hz); *m*: 5.53 (t, 7.6 Hz); *p*: 5.19 (t, 7 Hz)	Me: -1.16 (d, 6 Hz) and -1.55 (d, 5 Hz)[c]	Me: -1.12 (d, 6.4 Hz)[c]		

(a) in pyridine-d5
(b) partially overlaps with the solvent peak
(c) the C2-H was not located; we do not know why coordinated ^{i}PrNC gives two signals of 1:1 ratio.

2. Determination of the dissociation constant of (1Fe)$_2$ by serial dilution (Figure S3).

UV-vis spectra of (**1**Fe)$_2$ in toluene at 50 μM (black), 5 μM (red), 1 μM (blue), 0.5 μM (green) and 0.1 μM (purple) were measured. The resulting spectra were fitted using a least-squares protocol to a sum of the spectra of (**1**Fe)$_2$ and **2**Fe (Figure S2). The resulting molar fractions were fit to the equation: $xK_d/t_i = (1-2x)^2$, where x is the molar fraction of the dimer, t_i is the total concentration of Fe(por) moiety in the i^{th} dilution and K_d is the dissociation constant.

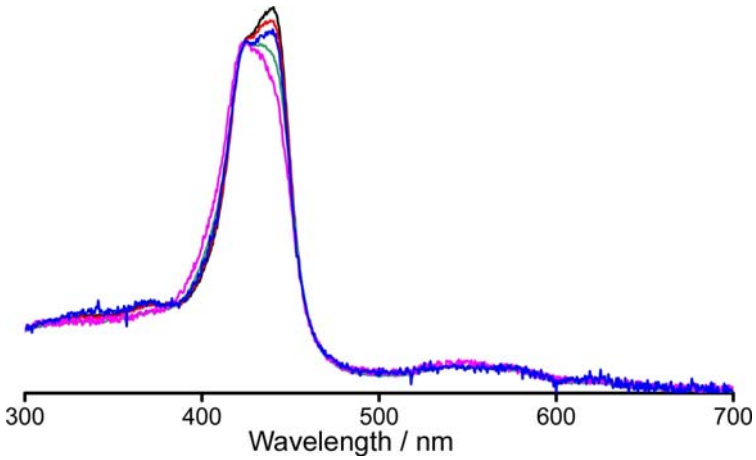

Figure S3. Serial dilution of toluene solutions of (**1**Fe)$_2$. All spectra are normalized to absorbance at 427 nm for illustrative purposes.

3. Spectrophotometric titrations.

Spectrophotometric titrations were performed in a drybox at 27±1 °C using a fiber optic dip probe with adjustable light path. Typically, a 10 μL aliquot of a stock solution of the ligand was added to a sample of the metalloporphyrin with stirring and two sequential scans were performed 1 min after the addition. We observed that the equilibrium establishes within <1 s after addition of the aliquot: the resulting spectra do not change over 30 min (in a sealed vial). The titration data for **2**Fe and **3**Fe was processes with SpecFit/32 software (Spectrum Software Associates). Titration data for (**1**Fe)$_2$ was processed using custom-written routine based on the least-squares fit of each absorption trace to a weighted sum of the spectra of (**1**Fe)$_2$ and (**1**Fe)$_2$L$_2$ (L = PhNO or *N*-MeIm) or (**1**Fe)$_2$, (**1**Fe)(^{i}PrNC) and (**1**Fe)$_2$(^{i}PrNC)$_2$ (for ^{i}PrNC titration). In titration with ^{i}PrNC, only the absorbance changes between 350 and 400 nm were used to build the Hill plots (Figure 2, main text) because in this range of wavelengths (**1**Fe)(^{i}PrNC) and (**1**Fe)$_2$(^{i}PrNC)$_2$ are indistinguishable, thereby allowing the separation of equilibria involving binding of ^{i}PrNC to the 5-coordinate ferroheme from the dissociation equilibrium. Titration curves, difference spectra and adduct spectra are shown in Figures S4-S9. The spectra of adducts (**1**Fe)$_2$L$_2$ (L = PhNO, *N*-MeIm and ^{i}PrNC) and of (**2**Fe)(PhNO) are compared in Figure S10.

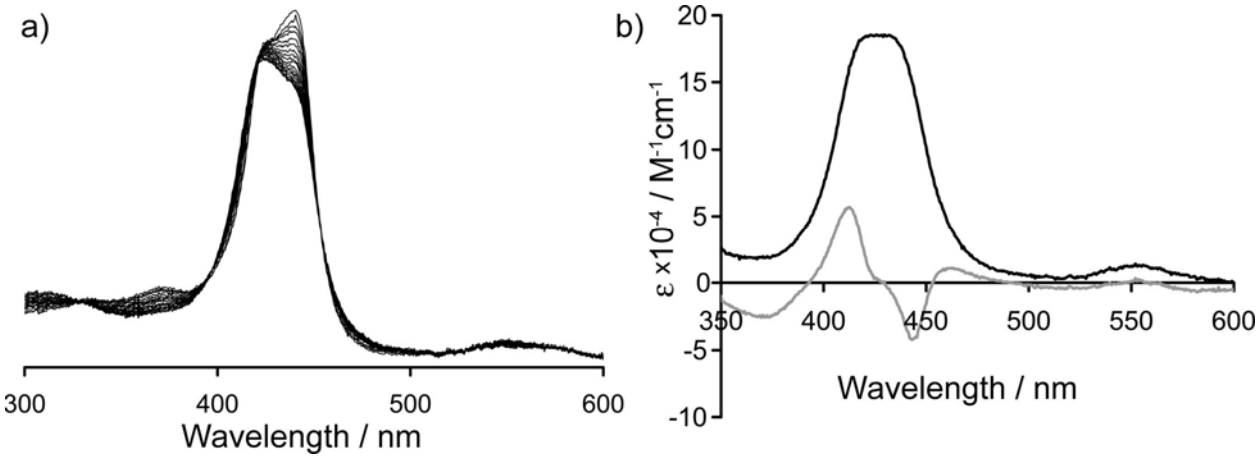

Figure S4. Results of spectrophotometric titration of (**1**Fe)$_2$ with PhNO in toluene; (a) typical series of titration curves, isosbestic points: 330, 394, 425, 457, 514, 582 nm; (b) spectrum of (**1**Fe)$_2$(PhNO)$_2$ (black) and the difference spectrum, (**1**Fe)$_2$(PhNO)$_2$ – (**1**Fe)$_2$ (grey).

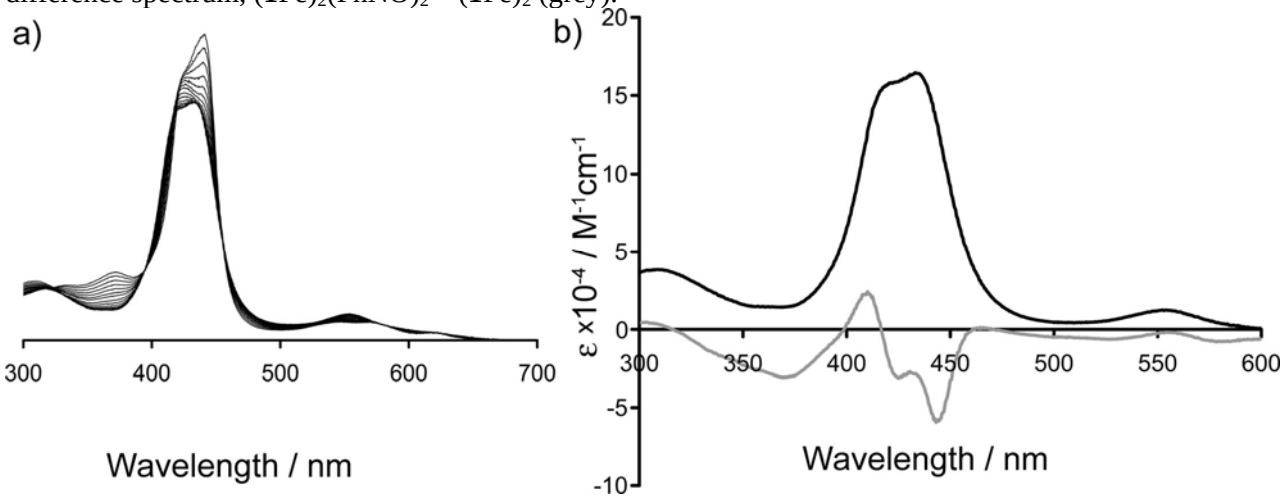

Figure S5. Results of spectrophotometric titration of (**1**Fe)$_2$ with *N*-MeIm in toluene; (a) typical series of titration curves, isosbestic points: 322, 396, 420, 455, 580, 620 nm; (b) spectrum of (**1**Fe)$_2$(N-MeIm)$_2$ (black) and the difference spectrum, (**1**Fe)$_2$(*N*-MeIm)$_2$ – (**1**Fe)$_2$ (grey).

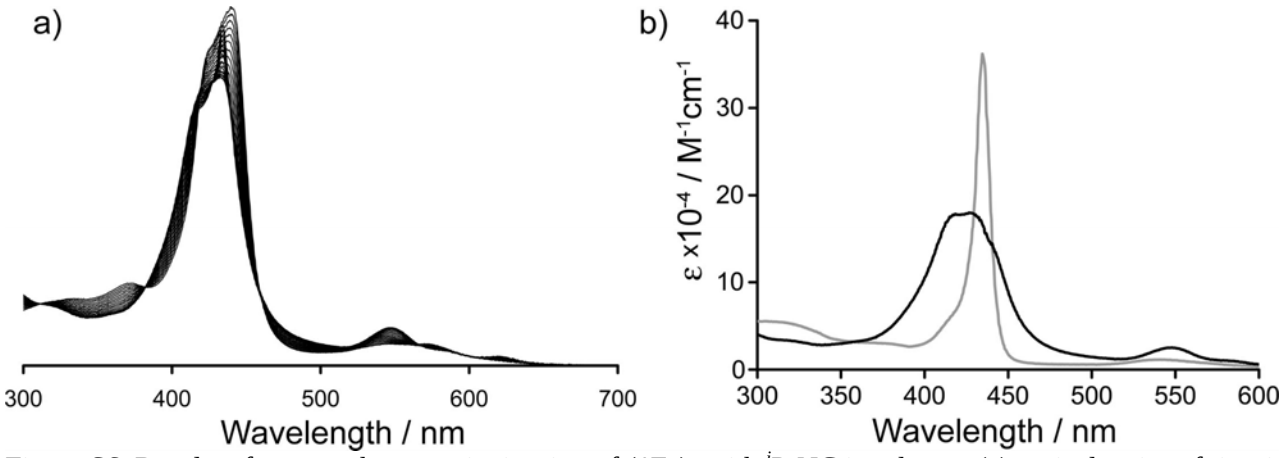

Figure S6. Results of spectrophotometric titration of (**1**Fe)$_2$ with ^{i}PrNC in toluene; (a) typical series of titration curves; (b) spectrum of (**1**Fe)$_2$(^{i}PrNC)$_2$ (black) and its monomer (**1**Fe)(^{i}PrNC).

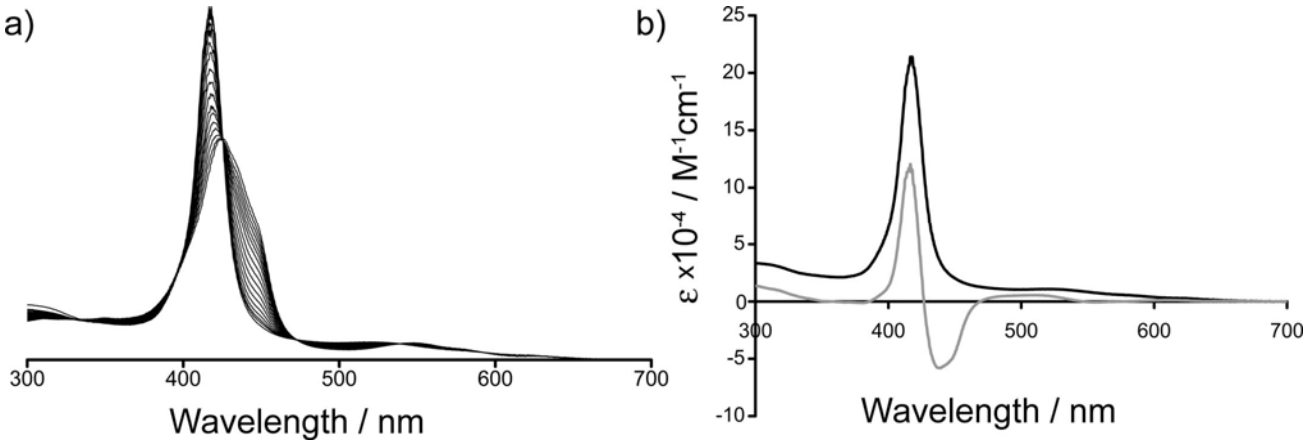

Figure S7. Results of spectrophotometric titration of **2**Fe with PhNO in toluene; (a) typical series of titration curves, isosbestic points: 334, 394, 425, 473, 540, 590 nm; (b) spectrum of (**2**Fe)(PhNO) (black) and the difference spectrum, (**2**Fe)(PhNO) – **2**Fe (grey). The spectra of **3**Fe are practically indistinguishable.

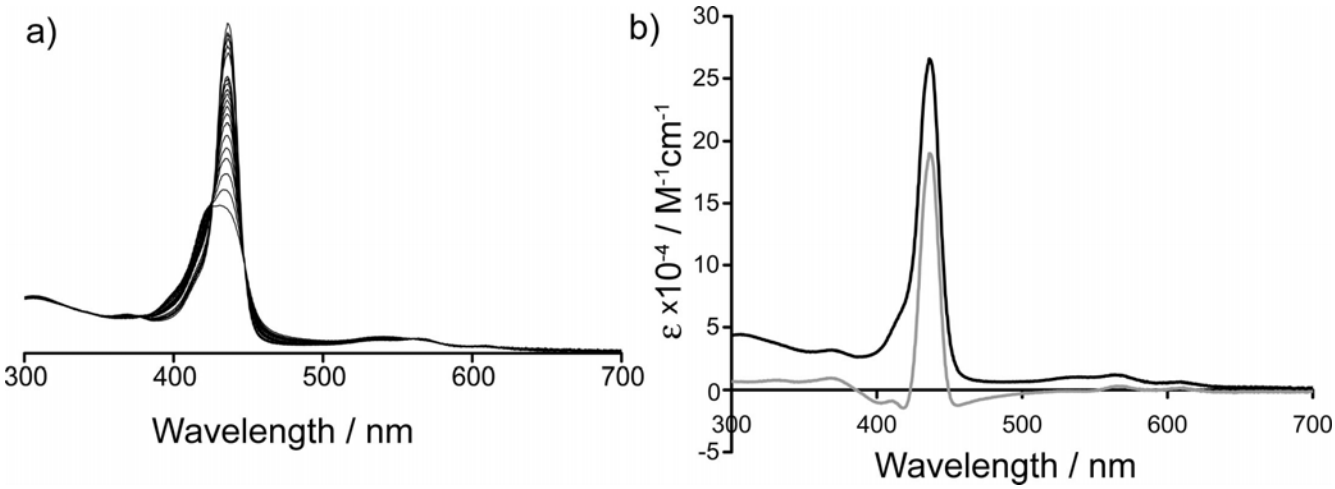

Figure S8. Results of spectrophotometric titration of **2**Fe with *N*-MeIm in toluene; (a) typical series of titration curves, isosbestic points: 355, 378, 427, 447, 558 nm; (b) spectrum of (**2**Fe)(*N*-MeIm) (black) and the difference spectrum, (**2**Fe)(*N*-MeIm) – **2**Fe (grey). The spectra of **3**Fe are practically indistinguishable.

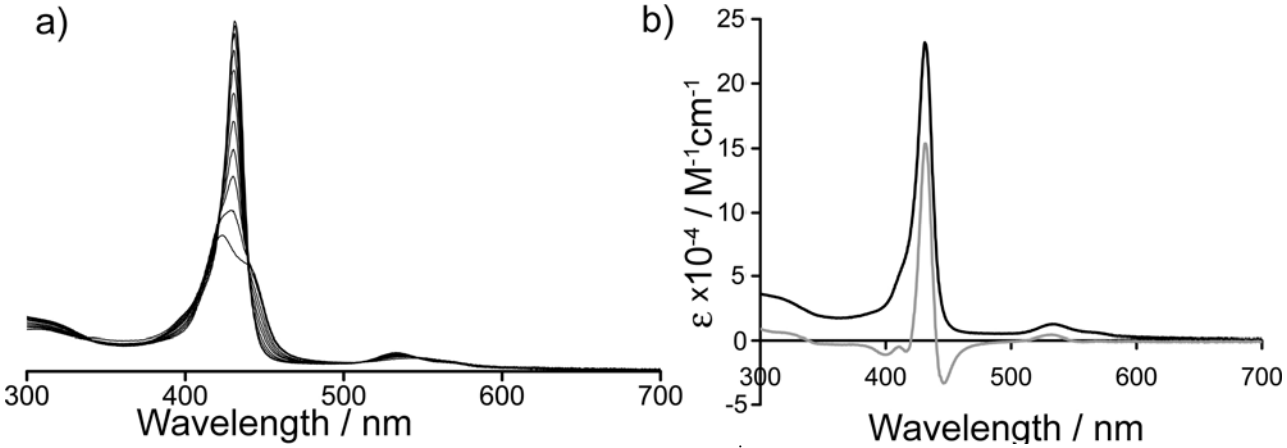

Figure S9. Results of spectrophotometric titration of **2**Fe with ^{i}PrNC in toluene; (a) typical series of titration curves, isosbestic points: 339, 419, 440, 506, 548 nm; (b) spectrum of (**2**Fe)(^{i}PrNC) (black) and the difference spectrum, (**2**Fe)(^{i}PrNC) – **2**Fe (grey). The spectra of **3**Fe are practically indistinguishable.

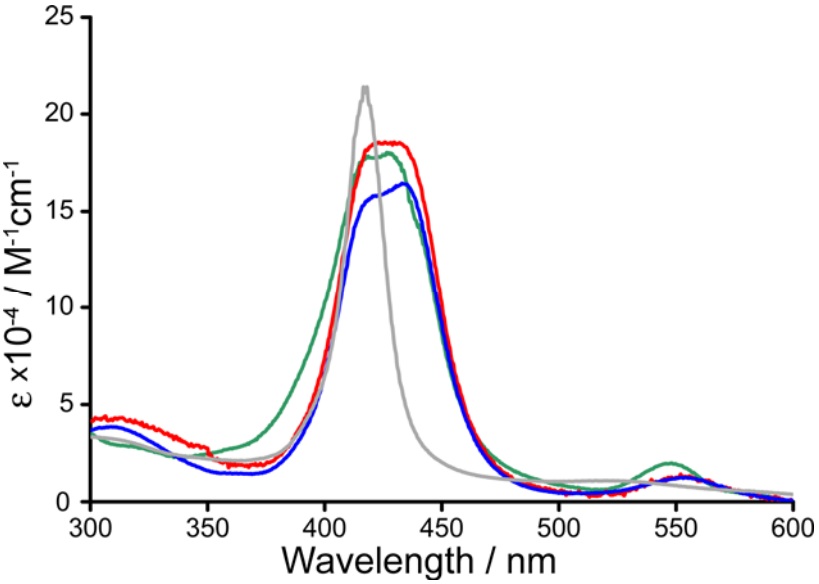

Figure S10. Comparison of absorption spectra of (**1**Fe)$_2$L$_2$, with L = PhNO (red), *N*-MeIm (blue) and ^{i}PrNC (green) and of **2**Fe(PhNO) (grey) to illustrate significant broadening of the Soret bands of the dimeric adducts.

4. Computations

All structure optimizations were carried out at the B3LYP/6-31g level with Gaussian03 software[2] using default convergence criteria. Unrestricted Kohn-Sham formalism was used in calculations for open-shell systems. Stability of wavefunctions was confirmed for all optimized structures. Following multiplicities were used in calculations for dimers:

Ligation state	Local multiplicity of Fe centers	Total multiplicity used in calculations	Notation
unligated	two "quintet" centers	nonet	$^{5+5}$**4**
	two "quintet" centers, antiferromagnetic	singlet, open-shell	$^{5-5}$**4**
monoligated	one "quintet" center, one "singlet" center	quintet	$^{5+1}$**4**(MeNC)
bisligated	two "singlet" centers	singlet, closed-shell	$^{1+1}$**4**(MeNC)$_2$

Computations for unligated dimers $^{5+5}$**4** and $^{5-5}$**4** were carried out with and without symmetry constraints. The highest symmetry point group enforced in calculations was C_s; however, structures after optimization in C_s symmetry were of C_{2h} symmetry within 0.01 Å tolerance. Symmetry was not restricted in computations for

[2] Gaussian03, Revision D.01. M. J. Frisch, G. W. Trucks, H. B. Schlegel, G. E. Scuseria, M. A. Robb, J. R. Cheeseman, J. Montgomery, J. A., T. Vreven, K. N. Kudin, J. C. Burant, J. M. Millam, S. S. Iyengar, J. Tomasi, V. Barone, B. Mennucci, M. Cossi, G. Scalmani, N. Rega, G. A. Petersson, H. Nakatsuji, M. Hada, M. Ehara, K. Toyota, R. Fukuda, J. Hasegawa, M. Ishida, T. Nakajima, Y. Honda, O. Kitao, H. Nakai, M. Klene, X. Li, J. E. Knox, H. P. Hratchian, J. B. Cross, V. Bakken, C. Adamo, J. Jaramillo, R. Gomperts, R. E. Stratmann, O. Yazyev, A. J. Austin, R. Cammi, C. Pomelli, J. W. Ochterski, P. Y. Ayala, K. Morokuma, G. A. Voth, P. Salvador, J. J. Dannenberg, V. G. Zakrzewski, S. Dapprich, A. D. Daniels, M. C. Strain, O. Farkas, D. K. Malick, A. D. Rabuck, K. Raghavachari, J. B. Foresman, J. V. Ortiz, Q. Cui, A. G. Baboul, S. Clifford, J. Cioslowski, B. B. Stefanov, G. Liu, A. Liashenko, P. Piskorz, I. Komaromi, R. L. Martin, D. J. Fox, T. Keith, M. A. Al-Laham, C. Y. Peng, A. Nanayakkara, M. Challacombe, P. M. W. Gill, B. Johnson, W. Chen, M. W. Wong, C. Gonzalez, J. A. Pople. **2004**, Wallingford, CT.

mono- and bis-ligated dimers to allow rotation of the $CNCH_3$ ligand. Resulting symmetries of the dimeric porphyrin core less the MeNC ligand(s) were C_s within 0.1 Å tolerance for $^{5+1}$**4**(MeNC) and C_{2h} within 0.01 Å for $^{1+1}$**4**$(MeNC)_2$.

Experimental and computed structural parameters for monomeric Fe(II) porphyrins are tabulated in Table S2; computed structural parameters for dimeric Fe(II) porphyrins are summarized in Table S3 and are shown in Figure S11.

The two Fe sites in the dimers are independent regardless of their spin and coordination state. Energy difference between the two states in either C_1 or C_s symmetry is not chemically significant (<0.1 kcal mol^{-1}); differences in structural parameters Fe-N_{Im} and Fe-Ct across all four structures ($^{5+5}$**4**, C_s; $^{5+5}$**4**, C_1; $^{5-5}$**4**, C_s; $^{5-5}$**4**, C_s) are within 0.003 Å. Upon ligand binding to one of the Fe sites structural parameters of the spectator site remain unperturbed regardless of its coordination and spin state (the largest change in structural parameters listed in Table S3 for spectator sites is 0.003 Å). Results of Mulliken population analysis show that the spin state of each Fe center in dimers depends only on its local coordination state.

Table S2. Experimental and calculated structural parameters for 5- and 6-coordinate monomeric Fe(II) porphyrins with imidazole (Im) and 2-methylimidazole (2-MeIm) ligands.

Complex	Ligand 1	Ligand 2	Fe-N_{Im}	Fe-Ct[a]	Fe-C (isocyanide)	Mulliken spin population
5-coordinate Fe^{II} porphyrin, exp. data	Im	-	2.131[b]	0.316[b]	-	quintet (4)
5-coordinate Fe^{II} porphyrin, exp. data	2-MeIm	-	2.150[c]	0.357[d]	-	
FeP, 5-coordinate quintet	Im	-	2.145	0.298	-	3.933
FeP, 5-coordinate quintet	2-MeIm	-	2.165	0.335	-	3.930
FeP, 6-coordinate singlet	2-MeIm	$CNCH_3$	2.125	0.007	1.827	0 (closed-shell)
FeP, 6-coordinate singlet	Im	$CNCH_3$	2.050	0.030	1.835	0 (closed-shell)
FeTPP, 6-coordinate singlet	Im	$CNCH_3$	2.049	0.033	1.834	0 (closed-shell)
6-coordinate Fe^{II} porphyrin, exp. data[e]	N-MeIm	CN-*i*Pr	2.039	0.024	1.847	singlet (0)

[a] Distance between Fe and the least-squares-plane defined by the four nitrogen atoms of the porphyrin ring.
[b] Average of reported values for Fe(II) porphyrins with various peripheral substituents coordinated with Im, Cambridge Structural Database (CSD) codes FUHVUZ[3] and GAJHAA.[4]
[c] Average of reported values for Fe(II) porphyrins with various peripheral substituents coordinated with 2-MeIm, CSD codes TALLEY,[5] TALLOI,[5] and SEHPOL.[5] Other structures (footnote *c*) have not been used due to disordered positions of the ligand.
[d] Average of reported values for Fe(II) porphyrins with various peripheral substituents coordinated with 2-MeIm, CSD codes MIYZUP,[6] PVPORI20,[7] TALLAU,[5] TALLEY,[5] TALLIC,[5] TALLOI,[5] SEHPOL,[8] SEHPUR,[8] and MAQLEW.[9]
[e] Reported crystal structure data for FeTPP ligated with N-MeIm and CN-*i*Pr, CSD code FATYEE.[10]

[3] S.J. Rodgers, C.A. Koch, J.R. Tate, C.A. Reed, C.W. Eigenbrot, W.R. Scheidt, *Inorg. Chem.* **1987**, *26*, 3647.
[4] M. Momenteau, W.R. Scheidt, C.W. Eigenbrot, C.A. Reed, *J. Am. Chem. Soc.* **1988**, *110*, 1207.
[5] C. Hu, A. Roth, M.K. Ellison, J. An, C.M. Ellis, C.E. Schulz, W.R. Scheidt, *J. Am. Chem. Soc.***2005**, *127*, 5675.
[6] M.K. Ellison, C.E. Schulz, W.R. Scheidt, *Inorg. Chem.***2002**, *41*, 2173.
[7] G.B. Jameson, F.S. Molinaro, J.A. Ibers, J.P. Collman, J.I. Brauman, E. Rose, K.S. Suslick, *J. Am. Chem. Soc.***1980**, *102*, 3224.
[8] C. Hu, J. An, B.C. Noll, C.E. Schulz, W.R. Scheidt, *Inorg. Chem.* **2006**, *45*, 4177.
[9] C. Hu, B. C. Noll, C.E. Schulz, W.R. Scheidt, *Inorg. Chem.* **2005**, *44*, 4346.
[10] R. Salzmann, M.T. McMahon, N. Godbout, L.K. Sanders, M. Wojdelski, E. Oldfield, *J. Am. Chem. Soc.***1999**, *121*, 3818.

Table S3. Selected experimental and calculated structural parameters for monomers and dimers with Fe(II) centers in various ligation states. Distances in Å.

Complex, spin state[a]	Fe-N_{Im}		Fe-Ct[b]		Fe-C (isocyanide)		Spin[c]		Energy, Hartree
	Fe1	Fe2	Fe1	Fe2	Fe1	Fe2	Fe1	Fe2	
$^{5+5}$**1**, C_s	2.170	2.169	0.358	0.358	-	-	3.936	3.936	-4953.54916776
$^{5+5}$**1**, C_1	2.168	2.168	0.358	0.358	-	-	3.937	3.937	-4953.54900827
$^{5-5}$**1**, C_s	2.167	2.168	0.359	0.360	-	-	-3.936	3.936	-4953.54902277
$^{5-5}$**1**, C_1	2.168	2.169	0.358	0.358	-	-	-3.937	3.937	-4953.54902277
$^{5+1}$**2**	2.167	2.158 [d]	0.355	0.007 [d]	-	1.823 [d]	3.936	0.000	-5086.24627386
$^{1+1}$**3**	2.161 [d]	2.161 [d]	0.009 [d]	0.009 [d]	1.822 [d]	1.822 [d]	0 [d] (closed-shell)	0 [d] (closed-shell)	-5218.94315496

[a] For unligated parallel dimers symmetry point group enforced in calculations is also noted. [b]Distance between Fe and the least squares plane defined by the four nitrogen atoms of the porphyrin. [c] From Mulliken spin population analysis.
[d] 6-coordinate centers.

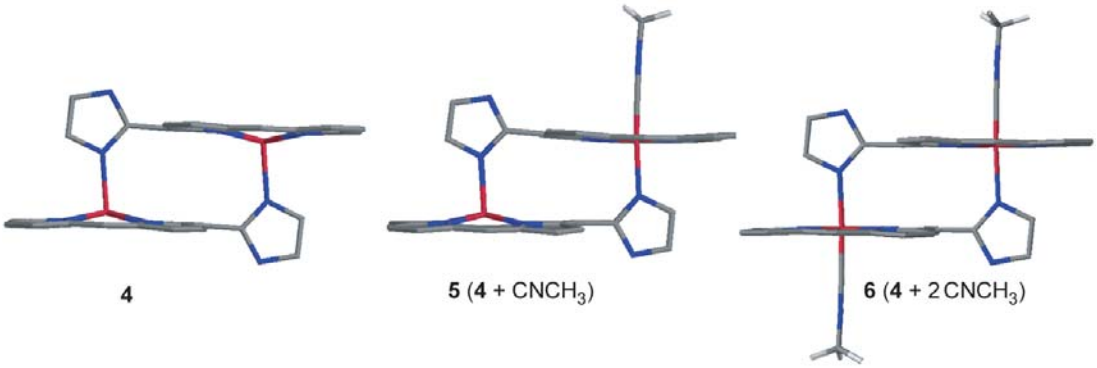

Figure S11. Computed structures of the model dimer 4 in the nonligated, monoligated and bisligated states with $CNCH_3$ ligands. Colors: Fe, red; C, grey; N, blue. Hydrogen atoms except for those of the $CNCH_3$ ligands are omitted for clarity.